Dynamics of Oligonucleotides Adsorbed on Thermosensitive Core−Shell Latex Particles

T. J. V. Prazeres, A. Fedorov, and J. M. G. Martinho*

Centro de Química-Física Molecular, Instituto Superior Técnico, Av. Rovisco Pais 1, 1049-001 Lisboa, Portugal

Received: March 5, 2004; In Final Form: April 20, 2004

The dynamics of a rhodamine X-labeled oligonucleotide composed of 25 mers of thymine (dT_{25}−ROX) in solution or adsorbed on the thermosensitive shell of poly(methyl methacrylate/*N*-isopropylacrylamide), poly-(MMA/NIPAM), core−shell nanoparticles, with a characteristic volume phase transition temperature (T_{VPT}) at ∼32 °C, were studied as a function of temperature by fluorescence anisotropy. The time-resolved anisotropy decay of the dT_{25}−ROX oligonucleotides in buffered solution (pH 5.5) is biexponential. The results are interpreted in terms of the "two-step" model, where the fast correlation time (θ_w) is attributed to the restricted "wobbling" motion of the bound ROX to the oligonucleotide (ODN) strand in a cone, while the slow correlation time (θ_{oligo}) is related to the rotation of the oligonucleotide as a whole. Both correlation times decrease with temperature due to the variation of the viscosity of the medium. The anisotropy decays of dT_{25}−ROX adsorbed on the PNIPAM thermosensitive shell were interpreted in terms of two models: the "*wobbling-in-two-cones*" and the *heterogeneous population* model. In both models, the fast correlation time is due to the "wobbling" motion of ROX (θ_w). The half-angle of the cone of the ROX "wobbling" motion (ϕ) decreases from ∼34° below the VPT to ∼11° above it, due to the increasing constraints imposed by the PNIPAM chains. The slow correlation time describes the overall rotational motion of the ODNs (θ_{oligo}) without restrictions (heterogeneous population model) or restricted to the "wobbling" in a cone ("wobbling-in-two-cones" model). The θ_{oligo} values of the adsorbed ODNs are higher than in solution and increase with temperature from ∼2.6 ns at 15 °C to reach a constant value of ∼6.6 ns after the transition due to the increasing friction by the PNIPAM chains. The anisotropy decay shows a residual component at long times (r_∞) that increases with temperature along the VPT, which is essentially due to the increasing percentage of immobilized ODNs from ∼14% at 15 °C to ∼70% above the transition (heterogeneous population model) or to the increase of the order parameter, S_{oligo}, with temperature from 0.38 ($\phi_{oligo} \sim 60°$) at 15 °C to 0.85 ($\phi_{oligo} \sim 27°$) at 45 °C ("wobbling-in-two-cones" model). Both models show that the whole motion of the ODNs and the randomization of their orientations are strongly restricted along the volume phase transition of the PNIPAM shell.

1. Introduction

Fluorescence polarization is a powerful tool to probe the dynamics of fluorophores in both homogeneous and heterogeneous media.[1−3] When a population of fluorophores is irradiated by linearly polarized light, those whose transition dipole moments are oriented in a direction close to the electric vector of the incident beam are preferentially excited (photoselection).[1,2] The emission of light from this population is anisotropic, and any molecular motion that changes the direction of the transition dipole moment leads to a decrease in the absolute value of the anisotropy and consequently to the depolarization of the fluorescence. One of the main mechanisms of fluorescence depolarization is the rotation of the probe during its lifetime. For free rotational Brownian motion the anisotropy decays to zero, but when the rotation is hindered a constant nonzero value is obtained at long times. This is caused by the fact that during the fluorescence decay, a random distribution of orientations is achieved for the free rotation but not when the rotational motion is hindered.[1−3] The fluorescence anisotropy provides the hydrodynamic volume of the isolated fluorophore[4] or that of the entity (protein,[5,6] polymer,[7] reversed micelle,[8] etc.) at which it is bound. It can also provide information about the internal segmental mobility of proteins,[9] polymers,[10] and other macromolecules.[11] Fluorescence anisotropy is widely applied to study the mobility of guest molecules in restricted environments such as micelles,[12−15] reversed micelles,[8,16−18] micellar aggregates,[19,20] lipid bilayers,[21] sol−gel silicates,[22] modified silica nanoparticles,[23] and double-stranded DNA.[24]

In the recent years, different polymeric nanoparticles have been developed for applications as supports.[25−28] They are particularly relevant in bioseparation, drug delivery, and diagnostics.[29,30] An interesting class of these materials are monodisperse core−shell latex particles of poly(methyl methacrylate/*N*-isopropylacrylamide), poly(MMA/NIPAM), which are structurally formed by a core of PMMA and a thermosensitive shell of PNIPAM. These thermosensitive materials can expand or contract on demand by changing the temperature around the volume phase transition temperature (T_{VPT}) of the PNIPAM shell. For aqueous dispersions, the T_{VPT} of the shell is approximately 32 °C,[31,32] which is identical to the lower critical solution temperature (LCST) of PNIPAM chains in water.[33] These core−shell particles can be used as supports in bioseparations and diagnostics, employing a recognition process between a probe in the shell (adsorbed or covalently linked) and the target biomolecule in solution.

The dynamics of terminal-labeled single-stranded ODNs (polythymine with 25 mers, dT_{25}) with rhodamine X, dT_{25}−

* To whom correspondence should be addressed. Fax: 351-21-8464455. Phone: 351-21-8419250. E-mail: jgmartinho@ist.utl.pt.

10.1021/jp0489931 CCC: $27.50
Published on Web 05/29/2004

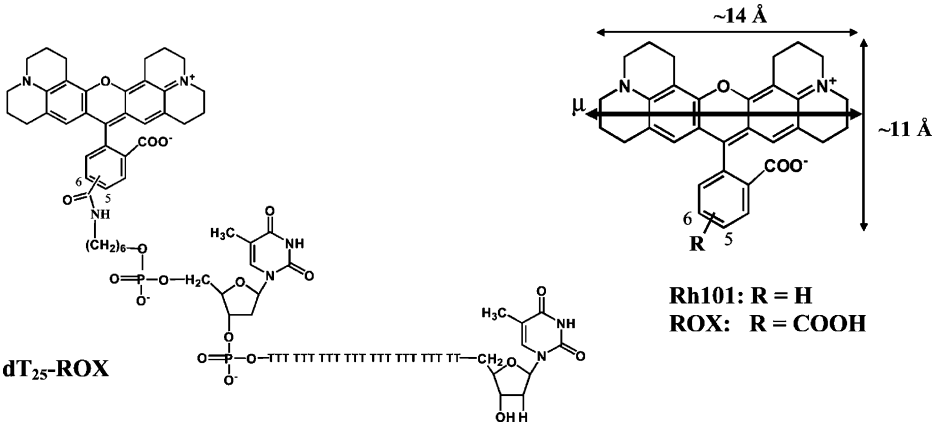

Figure 1. Molecular structures of the oligonucleotide with 25 mers of thymine labeled at the 5′-terminus with rhodamine X (dT_{25}−ROX), rhodamine 101 (Rh101), and rhodamine X (ROX). The bold arrow shows the direction of the $S_1 \leftarrow S_0$ electronic transition dipole moment, μ.

ROX, were studied by fluorescence anisotropy (time-resolved and steady-state) in solution or when adsorbed on the shell of the thermosensitive core−shell latex particles of poly(MMA/NIPAM). These results can be important when dealing with recognition processes, because the availability of the probe to the target should depend on the dynamics of the thermosensitive PNIPAM chains which influence the encounter between the "immobilized" probe in the particle and the target molecule in solution.

The results were interpreted with the help of the "wobbling-in-cone" model,[34−36] first introduced by Kinosita et al.[37] to describe the restricted diffusional motion of fluorescent dyes in lipid bilayers. The anisotropy of the labeled ODNs with rhodamine X (dT_{25}−ROX) in solution decays to zero at long times and shows both a slow and a fast correlation time due to the whole rotation of the ODN and to the restricted motion of the ROX bound to the ODN ("wobbling" motion), respectively. When adsorbed on the PNIPAM shell, the anisotropy decays at long times to a nonzero value due to orientational constraints imposed by the PNIPAM chains, which do not allow the randomization of orientations of the ODNs. These effects are enhanced by temperature increase along the volume phase transition. The fast relaxation time decreases continuously with temperature as in solution, while the slow relaxation time increases steeply near the T_{VPT}, due to the increasing friction from the PNIPAM chains. These results show that fluorescence anisotropy is an appropriate tool to probe the degree of restriction to the orientation and mobility of the adsorbed ODNs during the volume phase transition of the PNIPAM shell.

2. Experimental Section

Materials. The dT_{25}−ROX oligonucleotide, composed of 25 mers of thymine (dT_{25}) labeled at the 5′-terminus with rhodamine X (ROX), was purchased from ThermoHybaid in the lyophilized form (HPLC grade). Rhodamine 101 (Rh101, Radiant Dyes Chemie) was used without further purification. Their structures are shown in Figure 1.

The core−shell latex particles were synthesized and cleaned as reported elsewhere.[32] The solid content of the final latex dispersions is around 9.5 wt %. The diameter of the particles is ∼210 nm at room temperature and, due to the dehydration of the shell that induces the collapse of the PNIPAM chains, decreases to 160 nm above 35 °C.[32]

The shell volume phase transition occurs at ∼32 °C, which is close to the LCST of PNIPAM in water.

The dT_{25}−ROX oligonucleotides were dissolved in a buffer solution (pH 5.5 and ionic strength of 10 mM sodium chloride) to prepare a stock solution of 53 nmol/mL. The buffer solution (10 mM phosphate) was prepared using sodium dihydrogen phosphate 1-hydrate ($NaH_2PO_4 \cdot H_2O$, Panreac), disodium hydrogen phosphate (Na_2HPO_4, Riedel-de Haën), 10 mM sodium chloride (NaCl, Merck), and Milli-Q grade water. For fluorescence measurements 0.01 nmol/mL dT_{25}−ROX buffered solutions were prepared from the ODN stock solution. The samples containing latexes were very dilute (0.0125 wt % of latex) to avoid contamination of the fluorescence by Raleigh-scattered light. The concentration of oligonucleotide was adjusted, knowing the adsorption isotherms at 22 °C, to satisfy the condition that more than 95% of the ODNs are adsorbed.[32] The concentration of dT_{25}−ROX in solution is always less than 5.0×10^{-10} M. Before the measurements, the samples were incubated at room temperature (23 °C) for at least 3 h in order to guarantee the adsorption equilibrium.[27]

Fluorescence Spectra and Anisotropy. Steady-state fluorescence measurements were acquired in a SLM-AMINCO 8100 Series 2 spectrofluorimeter using 5 mm × 5 mm quartz cuvettes. The spectra were corrected for the response of the detection system, using the appropriate correction curve. For the steady-state anisotropy measurements, the sample is excited with vertically polarized light and the fluorescence-polarized components parallel ($I_{||}$) and perpendicular ($I_{\perp}$) to the direction of the excitation light were acquired. The steady-state anisotropy (r_{ss}) is then calculated by[1,2]

$$r_{ss} = \frac{I_{||} - GI_{\perp}}{I_{||} + 2GI_{\perp}} \quad (1)$$

where G is an instrumental correction factor, which takes into account the sensitivity of the monochromator to the polarization of the light. The intensities $I_{||}$ and $I_{\perp}$ were recorded using Glan-Thompson polarizers and corrected for the background. The excitation wavelength was 575 nm (8 nm bandwidth) while the emission wavelength was 615 nm (16 nm bandwidth). The temperature was controlled with a water circulating bath (±0.2 °C) from Julabo (model F25). The samples were kept at the desired temperature for 30 min under stirring before measurements.

Fluorescence and Anisotropy Decays. Time-resolved fluorescence intensity decays with picosecond resolution were obtained by the single-photon timing (SPT) technique using laser excitation at 575 nm. The system consists of a mode-locked

Coherent Inova 440-10 argon ion laser synchronously pumping a cavity-dumped Coherent 701-2 dye laser using rhodamine 6G, which delivers 5−6 ps pulses at a repetition rate of 1.9 MHz. The isotropic fluorescence decays were observed with a polarizer at the magic angle (54.7° to the direction of polarization of the excitation light), the Rayleigh-scattered light being effectively eliminated by a cutoff filter. The fluorescence was selected by a Jobin-Yvon HR320 monochromator with a grating of 100 lines/mm and detected by a Hamamatsu 2809U-01 microchannel plate photomultiplier.

The polarized fluorescence components parallel ($I_{||}$) and perpendicular ($I_{\perp}$) to the direction of polarization of the excitation light were also recorded. For our setup the correcting factor G is equal to 1, because the polarized fluorescence light components were depolarized before the entrance slit of the monochromator. The anisotropy by excitation with a δ-pulse of light is given by[1,2]

$$r(t) = \frac{I_{||}(t) - I_{\perp}(t)}{I_{||}(t) + 2I_{\perp}(t)} = \frac{I_{||}(t) - I_{\perp}(t)}{I(t)} \tag{2}$$

and the individual time-resolved fluorescence anisotropy components by[1,2]

$$I_{||}(t) = \frac{I(t)}{3}[1 + 2r(t)] \tag{3a}$$

$$I_{\perp}(t) = \frac{I(t)}{3}[1 - r(t)] \tag{3b}$$

where $I(t)$ and $r(t)$ are the fluorescence and the anisotropy decay curves for a δ-pulse excitation. The experimental decay curves were compared with the theoretical expressions obtained by δ-pulse excitation after being convoluted with the instrumental response function $g(t)$[38]

$$I_{exp}(t) = g(t) \otimes I(t) = \int_0^t g(\vartheta) I(t - \vartheta)\, d\vartheta \tag{4}$$

where $\otimes$ denotes the convolution integral.

The polarized fluorescence decay curves were globally fitted with eqs 3a and b, the lifetime of dT_{25}−ROX being fixed for each particular sample to its lifetime, and $r(t)$ approached by a sum of two exponentials, or a sum of two exponentials plus a constant, for the dT_{25}−ROX in solution or when adsorbed, respectively.

The fluorescence decay curves were fitted with homemade software that uses a nonlinear least-squares reconvolution method based on the Marquardt algorithm.[39] The goodness of the fit was judged from the distribution of residuals, the autocorrelation function, and the global χ^2 (lower than 1.2). To further confirm the fit procedure the steady-state anisotropy (r_{ss}) was calculated using the parameters obtained from the time-resolved analysis[1]

$$r_{ss} = \frac{\int_0^{\infty} I(t) r(t)\, dt}{\int_0^{\infty} I(t)\, dt} \tag{5}$$

and compared with the experimental steady-state anisotropy.[13]

3. Results

Rhodamine X was chosen as the fluorescence dye because of its excellent photophysical properties which are similar to those of the analogous rhodamine 101 (cf. Figure 1). The structural flexibility of the amino groups in these rhodamines is suppressed and their rotation hindered. This seems to be the main cause for their high quantum yields (~1) and monoexponential decays,[40−42] which are, in addition, almost temperature independent.[43−46] The fluorescence quantum yield of dT_{25}−ROX in water is 0.90 ± 0.05, slightly lower than 1.0, due to water quenching which seems to involve energy dissipation through the hydrogen bonds with the rhodamine.[32] In phosphate buffer solution (pH 5.5), the fluorescence decays of dilute solutions (~10^{-8} M) are monoexponential with lifetimes slightly changing from 4.9 ns at room temperature (22 °C) to 4.8 ns at 45 °C.[32] When adsorbed on the latex particles, the lifetime has an abrupt variation around the T_{VPT} of the PNIPAM shell, which was attributed to a sharp change of the refractive index, owing to the dehydration of the thermosensitive shell.[32] For temperatures far away from the T_{VPT} the dT_{25}−ROX lifetimes decrease with temperature in a similar way as that observed in solution.

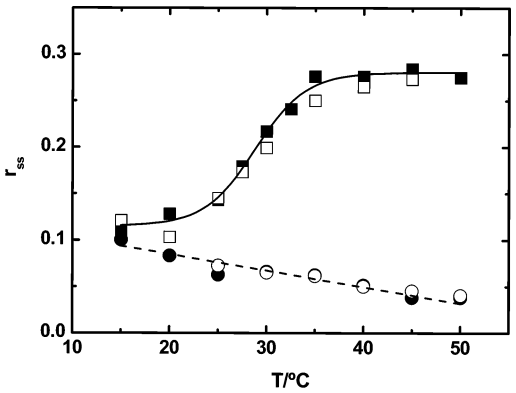

Figure 2. Plot of the steady-state anisotropy (r_{ss}) as a function of temperature in (●, ○) 10 mM phosphate buffer solution and ionic strength of 10 mM NaCl (10^{-8} M, pH 5.5) and (■, □) adsorbed on the core−shell latex particles (10^{-8} M, pH 5.5, 0.0125 wt % of latex particles). The filled symbols refer to experimental r_{ss}, while the open symbols refer to calculated r_{ss} values by eqs 10 and 13.

Figure 2 shows the steady-state anisotropy (r_{ss}) of dT_{25}−ROX in phosphate buffer solution and when adsorbed on the shell of the latex particles at several temperatures. In solution, r_{ss} decreases from 0.10 ± 0.02 at 15 °C to 0.04 ± 0.02 at 50 °C. The decrease of anisotropy with temperature is mostly due to the increase of the rotational diffusion coefficient of dT_{25}−ROX oligonucleotide with temperature. The anisotropy of dT_{25}−ROX was measured in very dilute latex dispersions (0.0125 wt % of latex), to avoid the contamination of the fluorescence by the scattered light. The experimental conditions were adjusted in order to ensure that more than 95% of the oligonucleotides are adsorbed. Thus, the anisotropy reports solely the dynamics of the oligonucleotides adsorbed on the thermosensitive shell. The average number of dT_{25}−ROX per particle was estimated to be around 120. This value was obtained from the ratio of concentrations of dT_{25}−ROX (~10^{-8} M) to particles (~8.5×10^{-11} M) in the dispersions. The molar concentration of particles was estimated from their mass concentration (~0.125 g/L), their volume at 45 °C (~2×10^{-21} m^3), and assuming that the density of the particles at this temperature (when the PNIPAM shell is collapsed) is identical to that of bulk PMMA (1.19 g/cm^3).[47] Despite the very low amount of dT_{25}−ROX per particle and the low concentration of particles, it was possible to obtain reasonable fluorescence intensities without the interference of scattered light.

Figure 2 shows that the steady-state anisotropy, r_{ss}, of the adsorbed dT_{25}−ROX as a function of temperature is distinct from that in solution. The r_{ss} values are always higher than those

TABLE 1: Fluorescence Decay and Rotational Dynamics Parameters for Rhodamine 101

T (°C)	τ, ns	θ, ps	η*, Pa·s	$1000 \cdot \theta T/\eta$, K·Pa^{-1}
23	4.12	179	9.33×10^{-4}	0.057
45	4.10	99	5.96×10^{-4}	0.053

*Viscosity of water.

in solution and increase with temperature, reaching a plateau (0.28 ± 0.02) for temperatures higher than 35 °C. At lower temperatures, the PNIPAM shell is well solvated by the water molecules; consequently the shell is very mobile and the water content is very high. The adsorbed dT_{25}−ROX oligonucleotides have enough freedom to move, behaving similarly to the oligonucleotide in solution (the r_{ss} values for dT_{25}−ROX in solution and adsorbed are very close at 15 °C). As the temperature increases, the shell begins to dehydrate, promoting attractive segmental interactions among the hydrophobic isopropyl groups of the polymer chain, which changes the chain conformation, resulting in the collapse of the PNIPAM chains at temperatures higher than 35 °C.[31,32,48] The volume phase transition (VPT) occurs around the LCST of PNIPAM in water (∼32 °C).[33] During the thermal transition, the shell dehydrates, its volume decreases, and the dynamics of the PNIPAM chains slow until reaching a globular conformation. Thus, the oligonucleotides become entrapped in this collapsed polymeric network, resulting in a drastic decrease in mobility with the consequent increase of the steady-state anisotropy. Above the transition, the conformation of the PNIPAM chains remains invariant and the r_{ss} values reach a plateau.

In order to obtain a quantitative insight about the dynamics of the labeled oligonucleotides (dT_{25}−ROX) in solution and when adsorbed, time-resolved fluorescence anisotropy measurements were performed.

The time-resolved anisotropy components of rhodamine 101 (Rh101), which is a reasonable model for ROX (cf. Figure 1), were initially recorded in the buffer solution at 23 and 45 °C to compare the differences in behavior between the labeled oligonucleotide and the free chromophore in solution. The Rh101 was excited at 575 nm which corresponds to the $S_1 \leftarrow S_0$ transition with the transition dipole moment aligned along the rhodamine's long axis (cf. Figure 1).[49] The fluorescence decay is monoexponential with lifetime $\tau = 4.1$ ns, irrespective of temperature. The anisotropy decay is also monoexponential, with rotational correlation time, θ, decreasing from 179 ps at 23 °C to 99 ps at 45 °C. These values agree with those reported for rhodamine B and rhodamine 6G in water.[8,50] The parameters obtained from the fittings are summarized in Table 1.

The hydrodynamic volume of Rh101 can be determined using the modified Debye−Stokes−Einstein (DSE) equation

$$V_H = \frac{A}{f}\frac{k_B T}{\eta}\theta \qquad (6)$$

where k_B is the Boltzmann constant, T the absolute temperature, η the viscosity of the solution, A the shape factor, and f the frictional coefficient. Recently, it has been reported by Dela Cruz and Blanchard that rhodamines closely obey the "stick" hydrodynamic boundary limit ($f = 1$) in polar solvents, and they have determined a shape factor of $A = 0.9$ for Rh101.[49] The apparent hydrodynamic volume of Rh101 of $V_H = 680$ Å^3 in phosphate buffer was calculated by the DSE model, knowing its rotational correlation time. This value is higher than the value calculated with the van der Waals increments,[51] which is $V_H^{calc} \approx 440$ Å^3. This behavior is commonly observed for protic solvents in which specific interactions such as hydrogen bonds are established between the solute and the surrounding solvent molecules, increasing the apparent hydrodynamic volume of the rotating unit.[52,53]

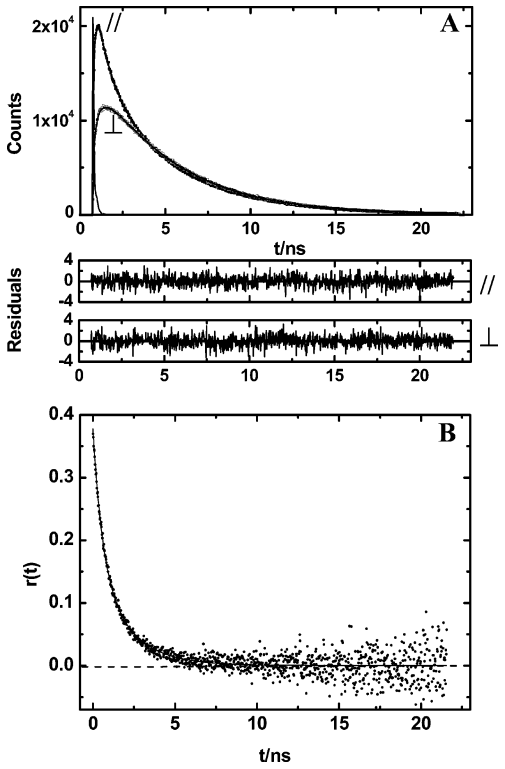

Figure 3. (A) Parallel (∥) and perpendicular (⊥) fluorescence decay components ($\lambda_{exc} = 575$ nm, $\lambda_{em} = 615$ nm) obtained for dT_{25}−ROX (10^{-8} M) in 10 mM phosphate buffer solution (pH 5.5) and ionic strength of 10 mM NaCl at 23 °C. The residuals for the parallel and perpendicular components globally fitted with eqs 8 ($\chi^2 = 1.03$) are also shown. (B) Fluorescence anisotropy decay. The solid line is the fitting curve using eq 9.

Figure 3 shows the parallel and perpendicularly polarized fluorescence decays (A) and the corresponding anisotropy (B) of dT_{25}−ROX in the phosphate buffer solution at 23 °C.

The anisotropy is well fitted with a sum of two exponentials[6,12,13,16]

$$r(t) = \beta_1 e^{-t/\theta_{slow}} + \beta_2 e^{-t/\theta_{fast}} \qquad (7)$$

with correlation times describing slow (θ_{slow}) and fast (θ_{fast}) dynamics and the sum of the preexponential factors being equal to the fundamental anisotropy, $r_0 = \beta_1 + \beta_2$. A similar behavior for labeled oligonucleotides with carboxytetramethylrhodamine (TAMRA) has been observed elsewhere.[54] Introducing eq 7 into eqs 3a and b and knowing that the fluorophore has a single-exponential decay $I(t) = a \exp(-t/\tau)$, we obtain

$$I_{\parallel}(t) = \frac{a}{3}[e^{-t/\tau} + 2\beta_1 e^{-t(1/\theta_{slow}+1/\tau)} + 2\beta_2 e^{-t(1/\theta_{fast}+1/\tau)}] \qquad (8a)$$

$$I_{\perp}(t) = \frac{a}{3}[e^{-t/\tau} - \beta_1 e^{-t(1/\theta_{slow}+1/\tau)} - \beta_2 e^{-t(1/\theta_{fast}+1/\tau)}] \qquad (8b)$$

Table 2 summarizes the parameters obtained by the global fit of the polarized parallel and perpendicular fluorescence decays with eqs 8a and b after convolution with the instrumental response function, the intrinsic lifetime being fixed to the value obtained from the isotropic fluorescence decay. Figure 3B shows

TABLE 2: Fluorescence Decay and Rotational Dynamics Parameters for dT_{25}−ROX in Phosphate Buffer Solution

T (°C)	τ, ns	θ_{slow}, ns[a]	θ_{fast}, ns	β_1	β_2	r_0	θ_w, ns	η, Pa·s[b]	$10^3 \cdot \theta_{oligo} T/\eta$, K Pa^{-1}	$10^3 \cdot \theta_w T/\eta$, K Pa^{-1}	S	ϕ, deg
23	4.90	2.00	0.58	0.17	0.21	0.38	0.82	9.33×10^{-4}	0.64	0.26	0.67	41
28	4.89	1.98	0.60	0.17	0.19	0.36	0.86	8.33×10^{-4}	0.71	0.31	0.69	39
30	4.88	1.96	0.54	0.15	0.22	0.37	0.75	7.98×10^{-4}	0.75	0.28	0.64	43
35	4.85	1.65	0.46	0.15	0.22	0.37	0.64	7.19×10^{-4}	0.71	0.27	0.63	43
40	4.83	1.72	0.45	0.10	0.27	0.37	0.61	6.53×10^{-4}	0.82	0.29	0.52	50
45	4.81	1.29	0.34	0.14	0.25	0.38	0.46	5.96×10^{-4}	0.69	0.24	0.60	45
50	4.72	1.07	0.29	0.15	0.23	0.38	0.39	5.47×10^{-4}	0.63	0.23	0.62	44

[a] $\theta_{slow} \approx \theta_{oligo}$. [b] Viscosity of water.

the experimental anisotropy fitted with the calculated anisotropy by eq 9,[55] fixing the values of the correlation times to those obtained before.

$$r_{exp}(t) = \frac{g(t) \otimes I(t) r(t)}{g(t) \otimes I(t)} \quad (9)$$

The preexponential factors (β_1, β_2) obtained from this fit are more accurate than those calculated from the global analysis of the polarized fluorescence decays, due to the correlation of parameters. The β_1 and β_2 values determined by this procedure are also reported in Table 2 for several temperatures.

The limiting anisotropy, r_0, is slightly lower than the predicted value of 0.4 for $S_1 \leftarrow S_0$ absorption and collinear transition dipole moments for absorption and emission. An experimental value of $r_0 = 0.37 \pm 0.01$ is obtained for dT_{25}−ROX in solution which is in agreement with the reported value of 0.373 ± 0.002 for xanthene derivatives.[56]

The steady-state anisotropy is also calculated by

$$r_{ss} = \frac{\beta_1 \theta_{slow}}{\theta_{slow} + \tau} + \frac{\beta_2 \theta_{fast}}{\theta_{fast} + \tau} \quad (10)$$

using the parameters recovered from the decay curve analysis. The calculated and the experimental steady-state anisotropy values are consistent at several temperatures (cf. Figure 2), confirming the adequacy of the fitting procedure.

For the samples with the dT_{25}−ROX adsorbed on the thermosensitive shell of the latex particles, a similar procedure was performed. Figure 4 shows the fluorescence depolarization decays (A) and the anisotropy (B) for a sample at 30 °C.

The anisotropy of the adsorbed dT_{25}−ROX does not decay to zero and can only be fitted with a sum of two exponentials plus a constant, according to[22b,c,23]

$$r(t) = \beta_1 e^{-t/\theta_{slow}} + \beta_2 e^{-t/\theta_{fast}} + r_\infty \quad (11)$$

where r_∞ is the anisotropy at long times ($t \rightarrow \infty$) and $r_0 = \beta_1 + \beta_2 + r_\infty$. The substitution of eq 11 into eqs 3a and b results in the following equations for the parallel and perpendicularly polarized decays, respectively.

$$I_{||}(t) = \frac{a}{3}[(1 + 2r_\infty)e^{-t/\tau} + 2\beta_1 e^{-t(1/\theta_{slow}+1/\tau)} + 2\beta_2 e^{-t(1/\theta_{fast}+1/\tau)}] \quad (12a)$$

$$I_{\perp}(t) = \frac{a}{3}[(1 - r_\infty)e^{-t/\tau} - \beta_1 e^{-t(1/\theta_{slow}+1/\tau)} - \beta_2 e^{-t(1/\theta_{fast}+1/\tau)}] \quad (12b)$$

The results of the fit are summarized in Table 3.

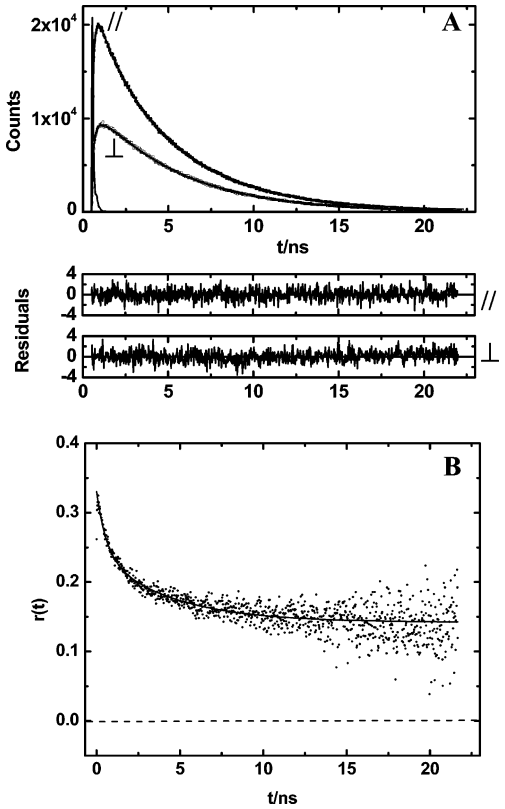

Figure 4. (A) Parallel (||) and perpendicular (⊥) fluorescence decay components ($\lambda_{exc} = 575$ nm, $\lambda_{em} = 615$ nm) obtained for dT_{25}−ROX (10^{-8} M) adsorbed on the core−shell latex particles (10^{-8} M, pH 5.5, 0.0125 wt % of latex particles) at 30 °C. The residuals for the parallel and perpendicular components globally fitted with eqs 12 ($\chi^2 = 1.05$) are also shown. (B) Fluorescence anisotropy decay. The solid line is the fitting curve using eq 9.

TABLE 3: Fluorescence Decay and Rotational Dynamics Parameters for dT_{25}−ROX Adsorbed on the Shell of the Thermosensitive Latex Particles

T (°C)	τ, ns	θ_{slow}, ns[a]	θ_{fast}, ns[b]	β_1	β_2	r_∞	r_0
15	4.88	2.77	0.64	0.195	0.150	0.033	0.378
23	4.86	2.54	0.60	0.154	0.165	0.032	0.350
25	4.83	3.88	0.70	0.108	0.140	0.079	0.327
28	4.82	3.99	0.61	0.108	0.132	0.109	0.350
30	4.80	4.30	0.57	0.100	0.088	0.142	0.331
35	4.61	5.55	0.41	0.099	0.034	0.194	0.327
40	4.60	6.32	0.36	0.094	0.024	0.209	0.327
45	4.57	6.61	0.41	0.087	0.016	0.220	0.323

[a] $\theta_{slow} \approx \theta_{oligo}$. [b] $\theta_{fast} \approx \theta_w$.

The limiting anisotropy of the adsorbed ODNs is $r_0 = 0.34 \pm 0.02$, which is slight lower than the value obtained for dT_{25}−ROX in the buffer solution ($r_0 = 0.37 \pm 0.01$), probably due to some residual scattering of the fluorescence by the latex particles.

As temperature increases, the anisotropy at long times (r_∞) increases, showing that the motion of ROX is hindered during its lifetime, preventing a complete fluorescence depolarization in that specific environment. The motion restriction increases with the temperature around the T_{VPT} of the PNIPAM shell.

To check the consistency of the results the steady-state anisotropy was calculated by

$$r_{ss} = \frac{\beta_1\theta_{slow}}{\theta_{slow}+\tau} + \frac{\beta_2\theta_{fast}}{\theta_{fast}+\tau} + r_\infty \qquad (13)$$

Figure 2 shows a good agreement between the experimental and calculated steady-state anisotropy values.

4. Discussion

Oligonucleotides (dT_{25}−ROX) in Solution. The fluorescence anisotropy $r(t)$, of the labeled oligonucleotide dT_{25}−ROX in solution can only be fitted with a sum of two exponentials. The results are explained by the "two-step" model[57] describing a slow and a fast motion. If those motions are uncorrelated, the global anisotropy is the product of the anisotropy of the slow (r_{slow}) and the fast (r_{fast}) motions[12,57,58]

$$r(t) = r_{slow}(t)\, r_{fast}(t) \qquad (14)$$

This model has been applied to describe the depolarization of dyes covalently attached to macromolecules[6,57] or within restricted media such as micelles,[12−14] reversed micelles,[8,16,17] and polymer−surfactant aggregates.[19]

It is not trivial to define the shape of the dT_{25}−ROX molecule due to the interplay of electrostatic interactions and stacking of the thymine bases by hydrophobic interactions and hydrogen bonding. Nevertheless, it seems that single-stranded ODNs adopt in aqueous solution a loose helical conformation[59] which can be described by the wormlike chain model.[60] However, if we assume that the oligonucleotide strand behaves as a spherical body ($f = 1$, $A = 1$), one can estimate the rotational correlation time for the whole oligonucleotide. Knowing the molecular volume of dT_{25}−ROX calculated with the van der Waals increments,[51] $V_H^{calc} \approx 6316$ Å^3, the rotational correlation time of the whole ODN was estimated by eq 6 as $\theta_{oligo} = 1.5$ ns. This value is lower than $\theta_{slow} = 2.0$ ns obtained experimentally for dT_{25}−ROX in solution at 23 °C (cf. Table 2), since we neglect the bound water, and the ODN molecule should be considered elongated despite its flexibility compared to a duplex strand. However, the closeness of these values justifies the attribution of the slow motion to the whole rotation of the ODN, although segmental motions of the ODN can also be present, despite its small contribution to the ROX depolarization due to the inherent rigidity of the dT_{25} strand.[60] The fast component of the anisotropy is due to the local motion of the ROX covalently bound by the hexyl tether to the ODN. This can be described by the "wobbling-in-cone" model as[12,14a,37,57]

$$r_{fast}(t) = r_0[S^2 + (1-S^2)e^{-t/\theta_w}] \qquad (15)$$

where S is the order parameter which gives an indication of the orientational distribution of the dye in equilibrium and θ_w is the orientational relaxation time of the "wobbling" motion. The "wobbling" motion of ROX is restricted, and consequently the randomization of orientations is not achieved, leading to a nonzero anisotropy at long times, $r_\infty = r_0S^2$.[12,36a,57] The rotational motion of the ODN as a whole is responsible for the decay of the anisotropy to zero. Indeed, the anisotropy of the slow rotation is given by

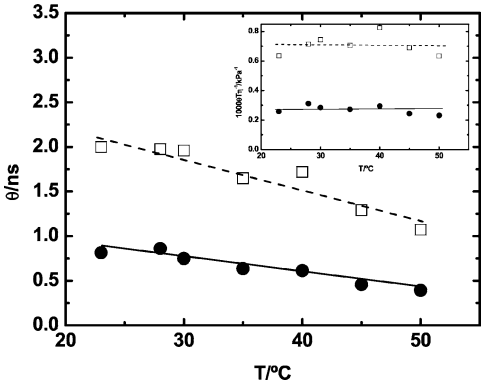

Figure 5. Temperature dependence of the rotational correlation times for the "wobbling" motion of ROX attached to the ODN strand (θ_w) and for the rotational diffusion of the whole oligonucleotide (θ_{oligo}) for oligonucleotides (dT_{25}−ROX) in 10 mM phosphate buffer solution (pH 5.5) and ionic strength of 10 mM NaCl. Inset: Corrected rotational correlation times for temperature and viscosity. Correlation times for the "wobbling" motion (●) and for the whole rotational diffusion (□).

$$r_{slow}(t) = e^{-t/\theta_{slow}} \qquad (16)$$

and then the global anisotropy (eq 14) is given by[12,13,14a,57]

$$r(t) = r_0[S^2e^{-t/\theta_{slow}} + (1-S^2)e^{-t/\theta_{fast}}] \qquad (17)$$

The slow correlation time $\theta_{slow} \approx \theta_{oligo}$, and then θ_{fast} is given by

$$\frac{1}{\theta_{fast}} = \frac{1}{\theta_w} + \frac{1}{\theta_{slow}} = \frac{1}{\theta_w} + \frac{1}{\theta_{oligo}} \qquad (18)$$

Figure 5 shows the plot of θ_{oligo} and θ_w as a function of temperature. Both decrease with temperature due to the increase of the diffusion rotational coefficient. Indeed, when the correlation times are multiplied by T/η, which takes into account the variation of the rotational diffusion coefficient with temperature and viscosity, a nearly constant value was obtained (see the inset of Figure 5).[61]

The preexponential factors in eq 7 are given by $\beta_1 = r_0S^2$ and $\beta_2 = r_0(1 - S^2)$. Then, the order parameter S can be calculated by $S^2 = \beta_1/(\beta_1 + \beta_2)$.[13,14a] For a "rod-shaped" molecule,[62,63] defined as a molecule in which the transition dipole moment is parallel to the long axis of the rotating unit (ODN molecule), the order parameter is given by[12,57]

$$S^2 = \left[\frac{1}{2}(\cos\phi)(1+\cos\phi)\right]^2 \qquad (19)$$

where ϕ is the half-angle of the cone of the "wobbling" motion. From eq 19, the possible values of S are in the range $0 \le |S| \le 1$. In the case of a "disk-shaped" molecule,[62,63] in which the excited dipole moment is perpendicular to the long axis of the rotating unit, the order parameter is given by[12,57]

$$S^2 = \left[\frac{1}{2}(1-\cos^2\phi)\right]^2 \qquad (20)$$

In this case, the probe has an equatorial "wobbling" motion. From eq 20, the possible values of S are in the range $0 \le |S| \le 0.5$.

The order parameters of dT_{25}−ROX in aqueous solution at different temperatures are shown in Table 2 and plotted in Figure

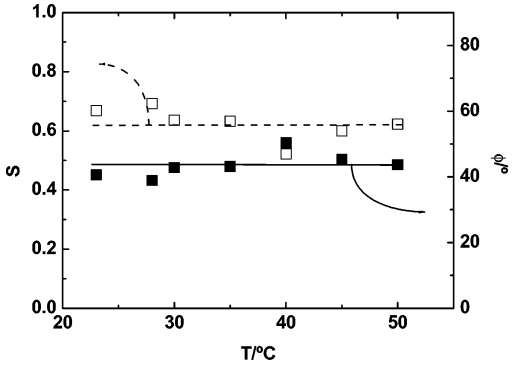

Figure 6. Plot of the order parameter (S) and the half-angle of the cone (ϕ) of the "wobbling" motion of ROX attached to the dT_{25} strand as a function of temperature in 10 mM phosphate buffer solution (pH 5.5) and ionic strength of 10 mM NaCl. (□) Order parameter; (■) half-angle of the cone.

6. The S values are constant with temperature; the average value is 0.61 ± 0.05. Furthermore, the values of S are higher than 0.5, and consequently the motion of the ROX attached to the oligonucleotide behaves more like a "rod-shaped" molecule,[12] with the transition dipole moment closely parallel to the long axis of the ODN. The half-angle of the cone ϕ was calculated by eq 19. Figure 6 shows that, irrespective of temperature, the values of ϕ are constant with an average value of 44° ± 3°.

Oligonucleotides (dT_{25}−ROX) Adsorbed on the Shell of the Latex Particles. The time-resolved anisotropy of the oligonucleotides adsorbed on the shell of the latex particles is more complicated than in solution. A residual anisotropy, r_∞, at long times is observed for the adsorbed oligonucleotides (cf. Figure 4 and Table 3), while in solution it is zero. This is a consequence of the hindered rotational diffusion of the ODNs when adsorbed that does not allow a complete randomization of the orientations. The anisotropy decays are well described by eq 11, with

$$\frac{1}{\theta_{slow}} = \frac{1}{\theta_{oligo}} + \frac{1}{\theta_{latex}} \tag{21}$$

$$\frac{1}{\theta_{fast}} = \frac{1}{\theta_{w}} + \frac{1}{\theta_{oligo}} + \frac{1}{\theta_{latex}} \tag{22}$$

θ_{latex} being the correlation rotational time of the latex particles. The rotational time of a sphere ($A = 1$, $f = 1$) in solution can be estimated by eq 6; knowing that the radius of the latex particle is 201 nm at 23 °C,[32] one obtains $\theta_{latex} \approx 0.97$ ms, and consequently $1/\theta_{latex} \approx 0$.

To explain the dynamics of the oligonucleotides adsorbed on the latex particles, we propose two models. One is a *heterogeneous population* model that considers two populations of adsorbed ODNs: the *mobile* ODNs which present a rotational diffusion similar to those in water and the *immobile* ODNs which do not have an overall rotation, and then their depolarization is simply due to the local "wobbling-in-cone" motion of ROX. Another possible model is the "*wobbling-in-two-cones*", in which the motions of the ROX and the whole ODNs are described by restricted "wobbling" motions in two distinct cones. Considering the heterogeneous population model, the anisotropy of the mobile ODNs is analogous to that of those in solution (eq 17), with $1/\theta_{slow} \approx 1/\theta_{oligo}$ and $1/\theta_{fast} \approx 1/\theta_{oligo} + 1/\theta_{w}$, and then

$$r_m(t) = r_0[S^2 + (1 - S^2)e^{-t/\theta_w}]\, e^{-t(1/\theta_{oligo})} \tag{23}$$

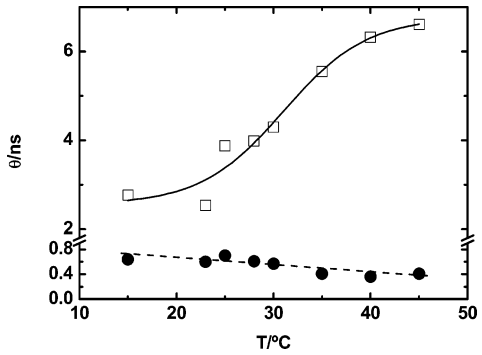

Figure 7. Temperature dependence of the rotational correlation times for the "wobbling" motion of ROX attached to the ODN strand (θ_w) and for the rotational diffusion of the whole oligonucleotide (θ_{oligo}) for oligonucleotides (dT25−ROX) adsorbed on the core−shell latex particles (10^{-8} M, pH 5.5, 0.0125 wt % of latex particles). Correlation times for the "wobbling" motion (●) and for the whole rotational diffusion (□).

The slow motion of the immobile ODNs in the PNIPAM shell is solely due to the rotation of the latex particle, and then $\theta_{oligo} \approx \theta_{latex} \approx \infty$. However, as the ROX continues to have its local motion of "wobbling-in-cone", its anisotropy is given by

$$r_{imm}(t) = r_0[S^2 + (1 - S^2)e^{-t/\theta_w}]\, e^{-t(1/\infty)} = r_0[S^2 + (1 - S^2)e^{-t/\theta_w}] \tag{24}$$

Considering α as the fraction of immobile ODNs, the total anisotropy is given by $r(t) = (1 - \alpha)r_m(t) + \alpha r_{imm}(t)$ and when $\theta_{oligo} \gg \theta_w$

$$r(t) = r_0(1 - S^2)e^{-t/\theta_w} + (1 - \alpha)r_0S^2e^{-t/\theta_{oligo}} + \alpha r_0S^2 \tag{25}$$

In the "wobbling-in-two-cones" model, the motion of the whole ODN is restricted to a cone with an order parameter S_{oligo}, and then the total anisotropy of dT_{25}−ROX is given by

$$r(t) = r_0[S^2 + (1 - S^2)e^{-t/\theta_w}][S_{oligo}{}^2 + (1 - S_{oligo}{}^2)e^{-t/\theta_{oligo}}] \tag{26}$$

If $\theta_{oligo} \gg \theta_w$, this equation simplifies to

$$r(t) = r_0(1 - S^2)e^{-t/\theta_w} + r_0(1 - S_{oligo}{}^2)S^2e^{-t/\theta_{oligo}} + r_0S^2S_{oligo}{}^2 \tag{27}$$

The comparison between eqs 25 and 27 with eq 11 shows that

$$\theta_w \approx \theta_{fast},\ \theta_{oligo} \approx \theta_{slow} \tag{28a}$$

$$\beta_1 = (1 - \alpha)r_0S^2, \qquad \beta_2 = r_0(1 - S^2), \qquad r_\infty = \alpha r_0S^2 \quad \text{(heterogeneous population)} \tag{28b}$$

$$\beta_1 = r_0(1 - S_{oligo}{}^2)S^2, \quad \beta_2 = r_0(1 - S^2), \quad r_\infty = r_0S^2S_{oligo}{}^2 \quad \text{("wobbling-in-two-cones")} \tag{28c}$$

Figure 7 shows the plot of θ_{oligo} and θ_w as a function of temperature. The θ_w values for the adsorbed oligonucleotide decrease with temperature as observed for the oligonucleotides in solution. This decrease is mostly due to the variation of local viscosity around the ROX probe with temperature. The values of θ_w for the adsorbed dT_{25}−ROX are slightly higher than in solution probably due to differences of the local viscosity of the hydrated shell compared to that in solution, or even to some constraints imposed by the PNIPAM chains. The values of θ_{oligo}

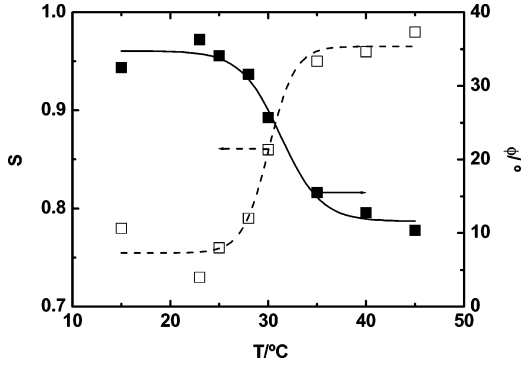

Figure 8. Plot of the (□) order parameter (S) and the (■) half-angle of the cone (ϕ) of the "wobbling" motion of ROX attached to the dT_{25} strand as a function of temperature, when dT_{25}−ROX is adsorbed on the core−shell latex particles (10^{-8} M, pH 5.5, 0.0125 wt % of latex particles).

TABLE 4: Rotational Parameters for dT_{25}−ROX Adsorbed on the Shell of the Thermosensitive Latex Particles

T (°C)	ϕ, deg	S	α	S_{oligo}	ϕ_{oligo}, deg
15	33	0.78	0.14	0.38	60
23	36	0.73	0.17	0.42	57
25	34	0.76	0.42	0.65	42
28	32	0.79	0.50	0.71	38
30	26	0.86	0.59	0.77	33
35	16	0.95	0.66	0.81	29
40	13	0.96	0.69	0.83	28
45	10	0.98	0.72	0.85	27

for the whole oligonucleotide increase with temperature from around 2.6 ns at 15 °C until ∼6.6 ns at 45 °C. The θ_{oligo} describe the overall rotational motion of the ODNs without restrictions (mobile ODNs in the heterogeneous population model) or restricted to the "wobbling" in a cone ("wobbling-in-two-cones" model). The unexpected increase of θ_{oligo} with temperature results from the friction imposed to the ODNs' motion by the continuous shrinking of PNIPAM chains that prevail over the decrease of aqueous medium viscosity, slowing down their motion.

The order parameter (S) for the local ROX motion within the cone was obtained at each temperature from eqs 28b,c. The order parameter and the corresponding half-angle of the cone (ϕ) values are summarized in Table 4 and shown in Figure 8. The order parameter increases from 0.75 ($\phi \sim 34°$) for temperatures below 25 °C to 0.97 ($\phi \sim 11°$) for temperatures above 35 °C. This indicates that the "wobbling" of ROX is strongly restricted by temperature increase along the VPT of the shell.

The time-resolved anisotropy does not decay to zero at long times but to a constant value r_∞ which increases with temperature (cf. Figure 4 and Table 3). In the heterogeneous population model this results from the fraction of immobile ODNs and the order parameter S of ROX "wobbling" (cf. eq 28b), while for the "wobbling-in-two-cones" model this is related to both restricted "wobbling" motions of the ROX and the ODN (cf. Equations 28c) which are characterized by the corresponding order parameters, S and S_{oligo}, respectively. For the heterogeneous population model the fraction of immobile ODNs (α) and the order parameter of the ROX restricted motion (S) were obtained from eq 28b, while for the "wobbling-in-two-cones" model the order parameters (S and S_{oligo}) were obtained from eq 28c. These values are summarized in Table 4.

The fraction of immobile ODNs (α) increase with temperature (cf. Figure 9). Indeed, at 15 °C, only ∼14% of the adsorbed oligonucleotides are immobile, increasing this fraction to ∼72% at 45 °C. This means that the changes in the PNIPAM shell drastically restrict the motion of the oligonucleotides at temperatures above the T_{VPT}.

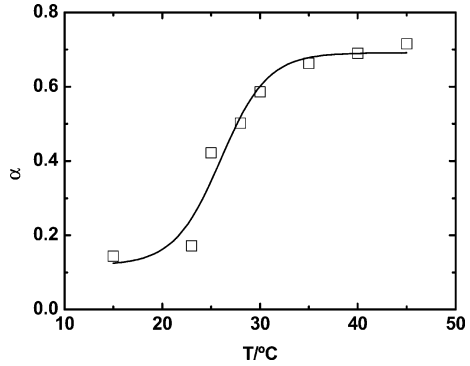

Figure 9. Temperature dependence of the immobile oligonucleotides fraction, for adsorbed dT_{25}−ROX oligonucleotides on the shell of the latex particles (10^{-8} M, pH 5.5, 0.0125 wt % of latex particles).

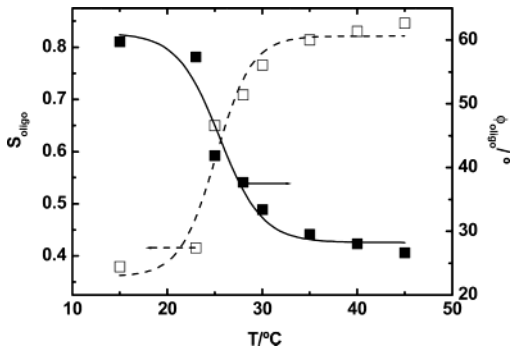

Figure 10. Plot of the (□) order parameter (S_{oligo}) and the (■) half-angle of the cone (ϕ_{oligo}) of the "wobbling" motion of the whole dT_{25}−ROX adsorbed on the core−shell latex particles as a function of temperature (10^{-8} M, pH 5.5, 0.0125 wt % of latex particles).

The values of S_{oligo} and the respective half-angles of the cone, ϕ_{oligo}, from the "wobbling-in-two-cones" model are plotted in Figure 10. The order parameter gives an indication of the amplitude of the diffusional motion of the whole oligonucleotide and then reflects the orientational constraints imposed by the PNIPAM chains of the shell particle. During the VPT, the PNIPAM shell collapses which limits the randomization of the adsorbed ODNs and results in the increase of S_{oligo} with temperature from 0.38 ($\phi_{oligo} \sim 60°$) at 15 °C to 0.85 ($\phi_{oligo} \sim 27°$) at 45 °C.

The two models predict a similar expression for the anisotropy decay, although based on distinct interpretation of the rotational behavior for the whole motion of the ODNs. The "wobbling-in-two-cones" model considers all the ODNs with a similar rotational diffusion within a cone without discriminating between mobile and immobile ODNs as does the heterogeneous population model. However, both models allow the characterization of the mobility of the adsorbed ODNs in the thermosensitive shell as a function of temperature, showing that the collapse of the PNIPAM chains slows down the rotational diffusion of the whole ODN and restricts the randomization of its orientations.

The dynamics of dT_{25}−ROX adsorbed on the shell of the thermosensitive nanoparticles are well correlated with the conformation changes of the PNIPAM chains. On the transition, the dynamics of the adsorbed oligonucleotides are strongly slowed and the randomization of their orientations restricted, reflecting the loss of mobility of the PNIPAM chains during the collapse of the shell. The increase of the steady-state

anisotropy, r_{ss}, with temperature (cf. Figure 2) is caused by the variation of several factors as can be seen from eq 13. However, the most important factor is the residual anisotropy, r_∞, that increases substantially with temperature along the volume phase transition, while the other terms in eq 13 vary slightly with temperature, or their contribution to r_{ss} is very small. This reflects the restrictions imposed by the PNIPAM chains to the whole motion of the oligonucleotide.

5. Conclusions

The results describe the dynamics of labeled single-stranded ODNs in solution and when adsorbed on the shell of poly(MMA/NIPAM) core−shell latex particles. The time-resolved fluorescence anisotropy of dT_{25}−ROX in phosphate buffer solution shows a fast and a slow correlation time. These were attributed to the "wobbling-in-cone" motion of ROX (θ_w) and to the whole rotation of the oligonucleotide (θ_{oligo}), respectively. The anisotropy decay of the oligonucleotides adsorbed on the positively charged PNIPAM shell of the latex particles shows both a fast and slow decay components and a residual anisotropy at long times (r_∞). The results were interpreted in terms of the "wobbling-in-two-cones" and the heterogeneous population model. In both models, the fast correlation time is due to the "wobbling" motion of ROX (θ_w). The half-angle of the cone of the ROX "wobbling" motion (ϕ) around the tether link to the ODN strand decreases from ∼34° ($S = 0.75$) below the VPT to ∼11° ($S = 0.97$) above it, due to the rise of the restrictions by the PNIPAM chains. The slow correlation time describes the overall rotational motion of the ODNs (θ_{oligo}) without restrictions (heterogeneous population model) or restricted to the "wobbling" in a cone ("wobbling-in-two-cones" model). The θ_{oligo} values increase from ∼2.6 ns at 15 °C below the VPT to attain a constant value of ∼6.5 ns above the VPT, due to the collapse of the PNIPAM shell which slows down the motion of the ODN. The residual anisotropy increases with temperature around the T_{VPT}, essentially due to the increase of the number of immobilized ODNs from ∼14% at 15 °C to ∼70% above the T_{VPT} in the heterogeneous population model or due to the increase of S_{oligo} with temperature from 0.38 ($\phi_{oligo} \sim 60°$) at 15 °C to 0.85 ($\phi_{oligo} \sim 27°$) at 45 °C in the "wobbling-in-two-cones" model. Both models lead to the conclusion that the whole motion of the ODNs and the randomization of their orientations are severely limited by the collapse of the PNIPAM chains.

Fluorescence anisotropy has been found to be an adequate tool to follow the dynamics of adsorbed oligonucleotides on the PNIPAM shell along the volume phase transition.

Acknowledgment. This work was supported by the "Fundação para a Ciência e a Tecnologia" (FCT), Portugal, under Project POCTI/1999/QUI/33866 and the Luso-French Scientific and Technical Cooperation Program. T. J. V. Prazeres acknowledges the FCT for the Ph.D. Grant SFRH/BD/5095/2001. The authors gratefully acknowledge Dr. A. Elaïssari (Unité Mixte CNRS-bioMérieux, ENS, Lyon) and A. M. Santos for providing the core−shell latex nanoparticles.

References and Notes

(1) Lackowicz, J. R. In *Principles of Fluorescence Spectroscopy*, 2nd ed.; Plenum Press: New York, 1999; Chapters 10 and 11.

(2) Valeur, B. In *Molecular Fluorescence. Principles and Applications*; Wiley-VCH: Weinheim, 2002; Chapter 5.

(3) Kalyanasundaram, K In *Photochemistry in Heterogeneous Systems*; Academic Press: Orlando, FL, 1987.

(4) (a) Dutt, G. B.; Srivatsavoy, V. J. P.; Sapre, A. V. *J. Chem. Phys.* **1999**, *111*, 9705. (b) Reed, W.; Politi, M. J.; Fendler, J. H. *J. Am. Chem. Soc.* **1981**, *103*, 4591.

(5) Heikal, A. A.; Hess, S. T.; Baird, G. S.; Tsien, R. Y.; Webb, W. W. *Proc. Natl. Acad. Sci. U.S.A.* **2000**, *97*, 11996.

(6) Martinho, J. M. G.; Santos, A. M.; Fedorov, A.; Baptista, R. P.; Taipa, M. A.; Cabral, J. M. S. *Photochem. Photobiol.* **2003**, *78*, 15.

(7) Paulo, P. M. R.; Gronheid, R.; De Schryver, F. C.; Costa, S. M. B. *Macromolecules* **2003**, *36*, 9135.

(8) Visser, A. J. W. G.; Vos, K.; van Hoek, A.; Santema, J. S. *J. Phys. Chem.* **1988**, *92*, 759.

(9) (a) Pandit, A.; Larsen, O. F. A.; van Stokkum, I. H. M.; van Grondelle, R.; Kraayenhof, R.; van Amerongen, H. *J. Phys. Chem. B* **2003**, *107*, 3086. (b) Rami, B. R.; Krishnamoorthy, G.; Udgaonkar, J. B. *Biochemistry* **2003**, *42*, 7986. (c) Tcherkasskaya, O.; Ptitsyn, O. B.; Knutson, J. R. *Biochemistry* **2000**, *39*, 1879.

(10) Jeon, S.; Bae, S. C.; Granick, S. *Macromolecules* **2001**, *34*, 8401.

(11) (a) Larsen, O. F. A.; van Stokkum, I. H. M.; Gobets, B.; van Grondelle, R.; van Amerongen, H. *Biophys. J.* **2001**, *81*, 1115. (b) Larsen, O. F. A.; van Stokkum, I. H. M.; Pandit, A.; van Grondelle, R.; van Amerongen, H. *J. Phys. Chem. B* **2003**, *107*, 3080.

(12) Quitevis, E. L.; Marcus, A. H.; Fayer, M. D. *J. Phys. Chem.* **1993**, *97*, 5762.

(13) Maiti, N. C.; Krishna, M. M. G.; Britto, P. J.; Periasamy, N. *J. Phys. Chem. B* **1997**, *101*, 11051.

(14) (a) Dutt, G. B. *J. Phys. Chem. B* **2002**, *106*, 7398. (b) Dutt, G. B. *J. Phys. Chem. B* **2003**, *107*, 3131. (c) Dutt, G. B. *J. Phys. Chem. B* **2003**, *107*, 10546. (d) Kelepouris, L.; Blanchard, G. J. *J. Phys. Chem. B* **2002**, *106*, 6600. (e) Kelepouris, L.; Blanchard, G. J. *J. Phys. Chem. B* **2003**, *107*, 1079.

(15) (a) Matzinger, S.; Hussey, D. M.; Fayer, M. D. *J. Phys. Chem.* **1998**, *102*, 7216. (b) Periasamy, N. *J. Fluoresc.* **2001**, *11*, 161. (c) DelaCruz, J. L.; Blanchard, G. J. *J. Phys. Chem. B* **2003**, *107*, 7102.

(16) Wittouck, N. W.; Negri, R. M.; De Schryver, F. C. *J. Am. Chem. Soc.* **1994**, *116*, 10601.

(17) Dutt, G. B. *J. Phys. Chem. B* **2004**, *108*, 805.

(18) (a) Willard, D. M.; Levinger, N. E. *J. Phys. Chem. B* **2000**, *104*, 11075. (b) Pant, D.; Levinger, N. E. *Langmuir* **2000**, *16*, 10123.

(19) Sen, S.; Sukul, D.; Dutta, P.; Bhattacharyya, K. *J. Phys. Chem. A* **2001**, *105*, 7495.

(20) Halder, A.; Sen, P.; Burman, A. D.; Bhattacharyya, K. *Langmuir* **2004**, *20*, 653.

(21) (a) Silvander, M.; Hansson, P.; Edwards, K. *Langmuir* **2000**, *16*, 3696. (b) Saito, H.; Minamida, T.; Arimoto, I.; Handa, T.; Miyajima, K. *J. Biol. Chem.* **1996**, *271*, 15515. (c) Lakowicz, J. R.; Prendergast, F. G. *Science* **1978**, *200*, 1399−1401. (d) Lakowicz, J. R.; Knutson, J. R. *Biochemistry* **1980**, *19*, 905. (e) Lakowicz, J. R.; Thompson, R. B. *Biochim. Biophys. Acta* **1983**, *732*, 359. (f) Pottel, H.; van der Meer, W.; Herreman, W. *Biochim. Biophys. Acta* **1983**, *730*, 181. (g) Lentz, B. R.; Barenholz, Y.; Thompson, T. E. *Biochemistry* **1976**, *15*, 4521. (h) Lentz, B. R.; Barenholz, Y.; Thompson, T. E. *Biochemistry* **1976**, *15*, 4529.

(22) (a) Ferrer, M. L.; del Monte, F.; Levy, D. *J. Phys. Chem. B* **2001**, *105*, 11076. (b) Flora, K. K.; Brennan, J. D. *J. Phys. Chem. B* **2001**, *105*, 12003. (c) Tleugabulova, D.; Zhang, Z.; Brennan, J. D. *J. Phys. Chem. B* **2003**, *107*, 10127.

(23) (a) Tleugabulova, D.; Duft, A. M.; Brook, M. A.; Brennan, J. D. *Langmuir* **2004**, *20*, 101. (b) Tleugabulova, D.; Zhang, Z.; Chen, Y.; Brook, M. A.; Brennan, J. D. *Langmuir* **2004**, *20*, 848.

(24) (a) Krishnamoorthy, G.; Duportail, G.; Mély, Y. *Biochemistry* **2002**, *41*, 15277. (b) Duhamel, J.; Kanyo, J.; Dinter-Gottlieb, G.; Lu, P. *Biochemistry* **1996**, *35*, 16687. (c) Madge, D.; Zappala, M.; Knox, W. H.; Nordlund, T. M. *J. Phys. Chem.* **1983**, *87*, 3286. (d) Millar, D. P.; Robbins, R. J.; Zewail, A. H. *J. Chem. Phys.* **1982**, *76*, 2080.

(25) Pichot, C.; Taniguchi, T.; Delair, T.; Elaïssari, A. *J. Dispersion Sci. Technol.* **2003**, *24*, 423.

(26) Nabzar, L.; Duracher, D.; Elaïssari, A.; Chauveteau, G.; Pichot, C. *Langmuir* **1998**, *14*, 5062.

(27) Ganachaud, F.; Elaïssari, A.; Pichot, C.; Laayoun, A.; Cros, P. *Langmuir* **1997**, *13*, 701.

(28) Charreyre, M. T.; Tcherkasskaya, O.; Winnik, M. A.; Hiver, A.; Delair, T.; Cros, P.; Pichot, C.; Mandrand, B. *Langmuir* **1997**, *13*, 3103.

(29) *Colloidal Biomolecules, Biomaterials, and Biomedical Applications*; Elaïssari, A., Ed.; Marcel Dekker: New York, 2003.

(30) Elaïssari, A.; Ganachaud, F.; Pichot, C. *Top. Curr. Chem.* **2003**, *227*, 169.

(31) Castanheira, E. M. S.; Martinho, J. M. G.; Duracher, D.; Charreyre, M. T.; Elaïssari, A.; Pichot, C. *Langmuir* **1999**, *15*, 6712.

(32) Prazeres, T. J. V.; Santos, A. M.; Martinho, J. M. G.; Elaïssari, A.; Pichot, C. *Langmuir*, in press.

(33) (a) Fujishige, S.; Kubota, K.; Ando, I. *J. Phys. Chem.* **1989**, *93*, 3311. (b) Kubota, K.; Fujishige, S.; Ando, I. *J. Phys. Chem.* **1990**, *94*, 5154.

(34) Kawato, S.; Kinosita, K. S.; Ikegami, A. *Biochemistry* **1977**, *16*, 2319.

(35) Kinosita, K. S.; Ikegami, A.; Kawato, S. *Biophys. J.* **1982**, *37*, 461.
(36) (a) Van Blitterswijk, W. J.; Van Hoeven, R. P.; Van Der Meer, B. W. *Biochim. Biophys. Acta* **1981**, *644*, 323. (b) Hildenbrand, K.; Nicolau, C. *Biochim. Biophys. Acta* **1979**, *553*, 365.
(37) Kinosita, K. S.; Kawato, S.; Ikegami, A. *Biophys. J.* **1977**, *20*, 289.
(38) O'Connor, D. V.; Phillips, D. In *Time-Correlated Single Photon Counting*; Academic Press Inc.: London, 1984; Chapter 2.
(39) Marquardt, D. W. *J. Soc. Ind. Appl. Math.* **1963**, *11*, 431.
(40) Karstens, T.; Kobs, K. *J. Phys. Chem.* **1980**, *84*, 1871.
(41) Arden, J.; Deltau, G.; Huth, V.; Kringel, U.; Peros, D.; Drexhage, K. H. *J. Lumin.* **1991**, *48* & *49*, 352.
(42) Kubin, R. F.; Fletcher, A. N. *J. Lumin.* **1982**, *27*, 455.
(43) Karpiuk, J.; Grabowski, Z. R.; De Schryver, F. C. *J. Phys. Chem.* **1994**, *98*, 3247.
(44) Vogel, M.; Rettig, W.; Sens, R.; Drexhage, H. *Chem. Phys. Lett.* **1988**, *147*, 452.
(45) Magde, D.; Rojas, G. E.; Seybold, P. G. *Photochem. Photobiol.* **1999**, *70*, 737.
(46) Barigelletti, F. *Chem. Phys. Lett.* **1987**, *140*, 603.
(47) Brandrup, J.; Immergut, E. H. *Polymer Handbook*, 3rd ed.; John Wiley & Sons: New York, 1989.
(48) Maeda, Y.; Higuchi, T.; Ikeda, I. *Langmuir* **2000**, *16*, 7503.
(49) Dela Cruz, J. L.; Blanchard, G. J. *J. Phys. Chem. A* **2002**, *106*, 10718.
(50) Klein, U. K. A.; Haar, H.-P. *Chem. Phys. Lett.* **1978**, *58*, 531.
(51) Edward, J. T. *J. Chem. Educ.* **1970**, *47*, 261.
(52) (a) Von Jena, A.; Lessing, H. E. *Chem. Phys.* **1979**, *40*, 245. (b) Von Jena, A.; Lessing, H. E. *Chem. Phys. Lett.* **1981**, *78*, 187.
(53) (a) Dela Cruz, J. L.; Blanchard, G. J. *J. Phys. Chem. A* **2001**, *105*, 9328. (b) Gumy, J.-C.; Vauthey, E. *J. Phys. Chem.* **1996**, *100*, 8628.
(54) Harley, M. J.; Toptygin, D.; Troxler, T.; Schildbach, J. F. *Biochemistry* **2002**, *41*, 6460.
(55) Berberan-Santos, M. N. *J. Lumin.* **1991**, *50*, 83.
(56) Johansson, L. B-A. *J. Chem. Soc., Faraday Trans.* **1990**, *86*, 2103.
(57) Lipari, G.; Szabo, A. *Biophys. J.* **1980**, *30*, 489.
(58) Lipari, G.; Szabo, A. *J. Am. Chem. Soc.* **1982**, *104*, 4546.
(59) Parkhurst, K. M.; Parkhurst, L. J. *Biochemistry* **1995**, *34*, 293.
(60) Murphy, M. C.; Rasnik, I.; Cheng, W.; Lohman, T. M.; Ha, T. *Biophys. J.* **2004**, *86*, 2530.
(61) Although the corrected values are nearly constant, the dependence of the correlation time for the "wobbling" motion is complex without a simple dependence on the viscosity of the medium.[13,57]
(62) Szabo, A. *J. Chem. Phys.* **1984**, *81*, 150.
(63) Edman, P.; Bergström, F.; Johansson, L. B-A. *Phys. Chem. Chem. Phys.* **2000**, *2*, 2795.